Laser & Photonics Reviews

LASER & PHOTONICS REVIEWS

www.lpr-journal.org

RESEARCH ARTICLE

Erbium-Doped Lithium Niobate-on-Insulator Waveguide Amplifier With 28 dB Fiber-to-Fiber Net Gain

Zhixuan Yu[1] | Liwen Deng[1] | Jing Qiu[1] | Feng Dang[1] | Jinli Han[2] | Tingting Ding[3] | Hao Li[1] | Yuanlin Zheng[1,4,5] | Xianfeng Chen[1,2,4,5]

[1]State Key Laboratory of Photonics and Communications, School of Physics and Astronomy, Shanghai Jiao Tong University, Shanghai, China | [2]Collaborative Innovation Center of Light Manipulations and Applications, Shandong Normal University, Jinan, China | [3]School of Electronic and Electrical Engineering, Shanghai University of Engineering Science, Shanghai, China | [4]Shanghai Research Center for Quantum Sciences, Shanghai, China | [5]Hefei National Laboratory, Hefei, China

Correspondence: Yuanlin Zheng (ylzheng@sjtu.edu.cn) | Xianfeng Chen (xfchen@sjtu.edu.cn)

Received: 28 April 2026 | **Revised:** 27 July 2026 | **Accepted:** 31 July 2026

Keywords: amplifier | lithium niobate | materials science | noise figure | optical amplifier | optical communication | optoelectronics | photonics | signal processing waveguide

ABSTRACT

High-gain optical amplifiers are critical for extending transmission capacity in optical communication and signal processing systems. We demonstrate a micro-waveguide amplifier based on an erbium-doped lithium niobate-on-insulator (Er:LNOI) platform. Under bidirectional pumping at 1480 nm, the amplifier achieves a fiber-to-fiber net gain exceeding 28 dB at 1531 nm with an input signal power of −25 dBm and a noise figure of 5.3 dB. The device also delivers a maximum output power exceeding 15 dBm. This fiber-to-fiber net gain represents the highest value reported for erbium-doped integrated waveguide amplifiers among all platforms to date, demonstrating that micro-waveguide geometry on the lithium niobate platform offers a promising architecture for high-gain amplifiers in integrated photonic systems.

1 | Introduction

Erbium-doped fiber amplifiers (EDFAs) have served as the foundation of global optical communication networks since the 1980s, providing high gain and low noise amplification [1–3]. The development of photonic integrated circuits (PICs) has stimulated growing interest in on-chip erbium-doped waveguide amplifiers (EDWAs), which inherit the low-noise characteristics of rare-earth gain media while offering compact footprints suitable for monolithic integration [4, 5]. Semiconductor optical amplifiers (SOAs) offer high integration density but suffer from pattern-dependent gain dynamics and high noise figures (NFs), limiting their use in noise-sensitive applications [6]. Various host materials have been explored for EDWAs, including silicon nitride, aluminum oxide, phosphate glass, tellurium oxide, and lithium niobate. Reported internal net gains range from several dB to over 30 dB, depending on waveguide length, doping concentration, and propagation loss [7–13].

Among these materials, Er:LNOI has attracted considerable attention as a multifunctional platform that combines efficient optical gain with the well-established advantages of lithium niobate, including strong electro–optic effect, excellent optical nonlinearity, and low propagation loss [5, 14–18]. The lithium niobate crystal lattice can accommodate erbium doping concentrations up to ∼0.5 mol%, enabling efficient interaction between light and erbium ions within compact waveguide geometries [19]. Recent demonstrations of Er:LNOI nano-waveguide amplifiers have achieved internal net gains of 16–38 dB in devices with lengths of 2.6–10 cm [20–24], and fiber-to-fiber net gains up to 18 dB have been realized using high-efficiency edge couplers [25]. However, further enhancement of the fiber-to-fiber net gain remains critical for practical system deployment. Compared with nano-waveguides, micro-waveguide designs provide better mode matching with standard optical fibers and higher power handling capability because of their larger effective mode areas.

In this work, we design an Er:LNOI waveguide amplifier with a microscale geometry and an extended gain length, achieving a record external net gain. By serially connecting two Er:LNOI micro-waveguide segments, we achieve a total gain length of 11.2 cm while maintaining single-mode operation under bidirectional pumping at 1480 nm. The amplifier delivers a record fiber-to-fiber net gain exceeding 28 dB at 1531 nm with an input signal power of −25 dBm, the highest value among erbium-doped integrated waveguide amplifiers, along with an output power exceeding 15 dBm and an NF of 5.3 dB.

2 | Results

2.1 | Device Design and Fabrication

The micro-waveguide amplifier is fabricated on a 3-inch x-cut Er:LNOI wafer comprising a 5 μm thick Er:LN film, a 2 μm thick buried oxide layer, and a silicon substrate. The erbium doping concentration is approximately 0.5 mol%. The Er:LN film is prepared from an as-grown Er:LN crystal by the Czochralski method. The Er:LN crystal was bonded on top of the buried oxide layer and chemo-mechanically thinned to the designed thickness. Figure 1a illustrates the amplifier configuration, where two waveguide chips are precisely aligned in series to provide a total gain length of 11.2 cm. The ridge waveguides are patterned by UV lithography using a thick photoresist layer, followed by inductively coupled plasma reactive ion etching (ICP-RIE) with argon ion milling [26]. The top width is 4 μm, and the etching depth is 2 μm with a sidewall angle of about 60°, resulting in a waveguide cross-section of approximately 6 μm × 5 μm. Following etching, a tantalum pentoxide cladding layer with a thickness of approximately 0.8 μm is deposited by sputtering. Subsequently, all the waveguide facets are polished at an angle of 5.2° to suppress back reflection and thereby prevent parasitic lasing. The simulated fundamental TE mode profile is overlaid on the scanning electron microscope (SEM) cross-sectional image of the waveguide in Figure 1b, showing that the fundamental TE mode is well confined within the erbium-doped region.

The micro-waveguide geometry is specifically designed for compatibility with standard lensed fibers, giving a measured coupling loss of 1.78 dB per facet. Compared to nano-waveguides commonly employed in integrated photonics, the larger mode area of our microscale design offers enhanced power handling capability and reduced optical intensity, which helps mitigate nonlinear impairments such as excited-state absorption (ESA) and cooperative upconversion at high pump powers [27]. The three-dimensional spatial distribution of erbium ions within the lithium niobate crystal, characterized by time-of-flight secondary ion mass spectrometry (TOF-SIMS), is presented in Figure 1c. The results reveal a homogeneous doping profile over a depth of 1 μm, confirming a uniform erbium distribution throughout the probed waveguide volume. From the TOF-SIMS data, the erbium doping concentration is calculated to be 0.47 mol%.

The fluorescence lifetime of the metastable $^4I_{13/2}$ energy level is a critical parameter that determines the energy storage capacity and gain dynamics of the Er:LNOI waveguide amplifier. In the erbium three-level energy system, pump photons at 1480 nm excite Er^{3+} ions from the $^4I_{15/2}$ ground state to the $^4I_{13/2}$ metastable state, from which stimulated emission at the signal wavelength occurs. The fluorescence lifetime is measured by time-resolved photoluminescence spectroscopy, where the decay of the emission intensity is recorded after pulsed excitation. The measured fluorescence lifetime of the $^4I_{13/2}$ metastable level is 2.42 ms, as illustrated in Figure 1d, consistent with values reported for erbium-doped lithium niobate at similar doping concentrations [19].

Estimated from the top-view intensity of the scattered fluorescence at 1480 nm as depicted in Figure 1e, the propagation loss is fitted to be 0.37 dB/cm. This value includes both the waveguide scattering loss and Er^{3+} absorption. The coupling loss is then derived by subtracting the total propagation loss from the measured insertion loss, yielding a coupling loss of 1.78 dB per facet. The connection loss between the two EDWA chips is then estimated to be 4.43 dB.

2.2 | Amplification Characteristics and Theoretical Analysis

The experimental setup for characterizing the Er:LNOI waveguide amplifier is illustrated in Figure 2a. A tunable laser source provides the input signal at 1531 nm, whose power and polarization are adjusted by an electrically variable optical attenuator (EVOA) and controlled by a polarization controller (PC) before being combined with the 1480-nm pump light through a wavelength division multiplexer (WDM). The polarization controllers in the signal and pump paths are used for input polarization adjustment, to ensure fundamental TE modes are excited in the Y-propagating waveguide chip. For the X-cut, Y-propagating waveguides, these modes are predominantly π-polarized along the crystallographic z axis [28]. The two Er:LNOI waveguide chips are placed in close proximity and coupled in series, with lensed fibers coupled to the input and output facets for signal injection and extraction, as shown in the inset of Figure 2a. Bidirectional pumping at 1480 nm is employed to achieve uniform population inversion along the total length. The WDM at the output side serves two purposes: it provides the backward pump injection path for bidirectional pumping, and separates the amplified signal from the residual pump light for analysis by the optical spectrum analyzer (OSA).

Figure 2b illustrates the fiber-to-fiber net gain and output power as a function of the input signal power at 1531 nm. At an input power of −25 dBm, the amplifier achieves a fiber-to-fiber net gain of 28.2 dB. This represents the highest directly measured fiber-to-fiber net gain among erbium-doped integrated waveguide amplifiers. The fiber-to-fiber net gain, also referred to as external net gain, is the power gain directly measured between the input and output fibers, with all losses along the optical path included. As the input signal power increases, the net gain gradually decreases due to gain saturation, while the output power continues to rise until reaching a maximum of 15.8 dBm [29]. Table 1 compares our device with other platforms, showing higher off-chip net gain

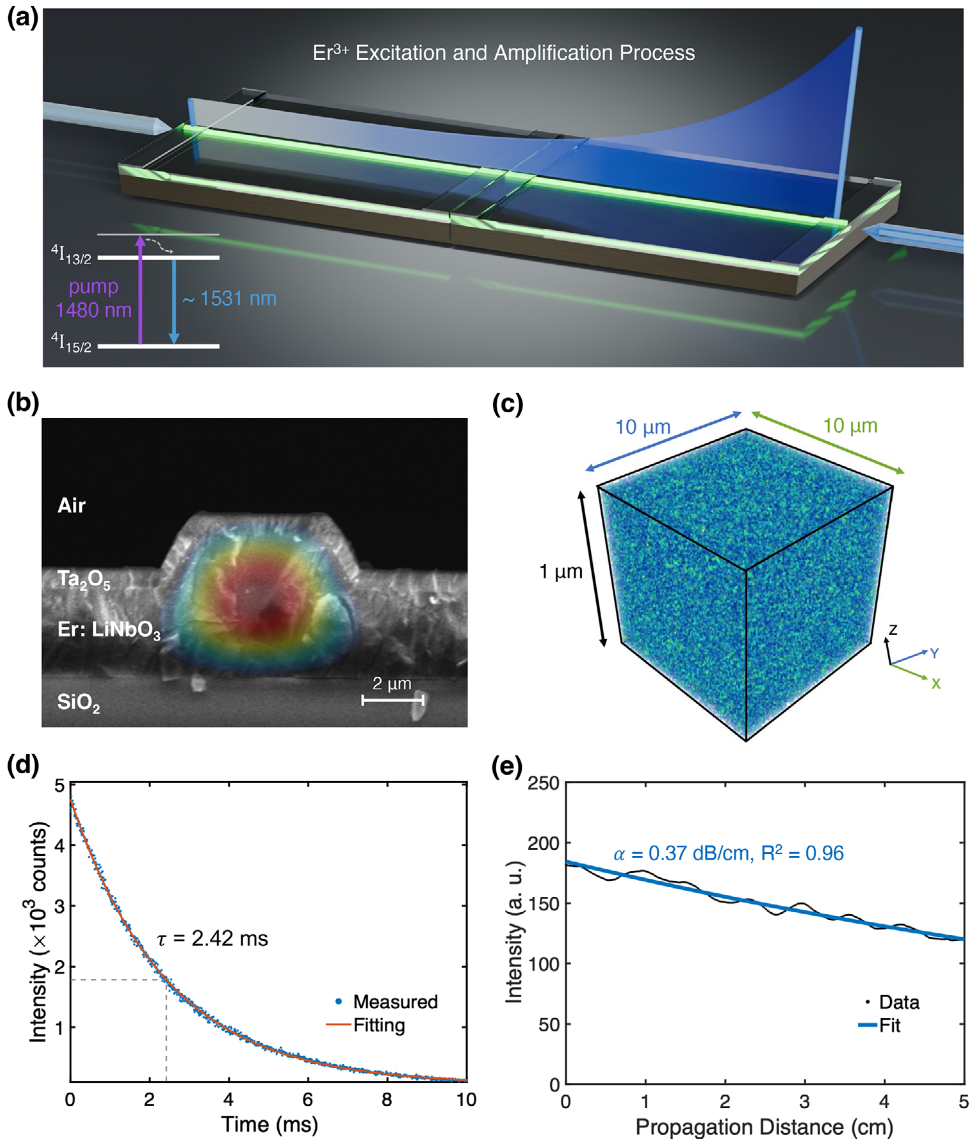

FIGURE 1 | Device design, material characterization, and waveguide properties. (a) Schematic of the Er:LNOI waveguide amplifier with two waveguide segments aligned in series. Inset: energy level diagram of the 1480 nm pumping scheme. (b) Scanning electron microscope (SEM) cross-sectional image of the ridge waveguide overlaid with the simulated fundamental TE mode profile. (c) Three-dimensional distribution of erbium ions in the lithium niobate crystal measured by TOF-SIMS. (d) Fluorescence lifetime measurement of the $^4I_{13/2}$ metastable level, yielding $\tau = 2.42$ ms. (e) Propagation loss measurement by scattered fluorescence light from top-view imaging.

and output power. Furthermore, the dependence of the fiber-to-fiber net gain and NF on the total pump power is depicted in Figure 2c. The net gain increases rapidly before reaching saturation, while the NF stabilizes at approximately 5.3 dB under optimal pumping conditions. Throughout our characterization, the experimental data are consistent with theoretical simulations based on a three-level rate equation model that accounts for mode overlap, ground-state absorption, stimulated emission, ESA, and propagation losses.

Figure 2d displays the input and output spectra of the amplifier at an input signal power of −25 dBm, where a signal enhancement of over 28 dB is clearly observed at 1531 nm along with the ASE background across the C-band. To examine the dependence of gain on device length and pump power, we simulate the net gain as a function of both parameters, as shown in the contour plot of Figure 2e. The simulation predicts that higher gains can be achieved with longer waveguides and higher pump powers. However, beyond the optimal length, further increasing the waveguide length does not significantly improve the net gain, as signal reabsorption by erbium ions can occur when pump depletion leads to insufficient inversion in the rear section of the waveguide. A more scalable route to longer gain lengths is to realize a spiral gain waveguide on a single chip. Reducing the refractive-index contrast between the Er:LN core and substrate could lead to weaker optical confinement and fewer supported modes. With appropriate bend optimization, this design with fewer supported modes could enable low-loss spiral routing while retaining a large mode area for fiber coupling.

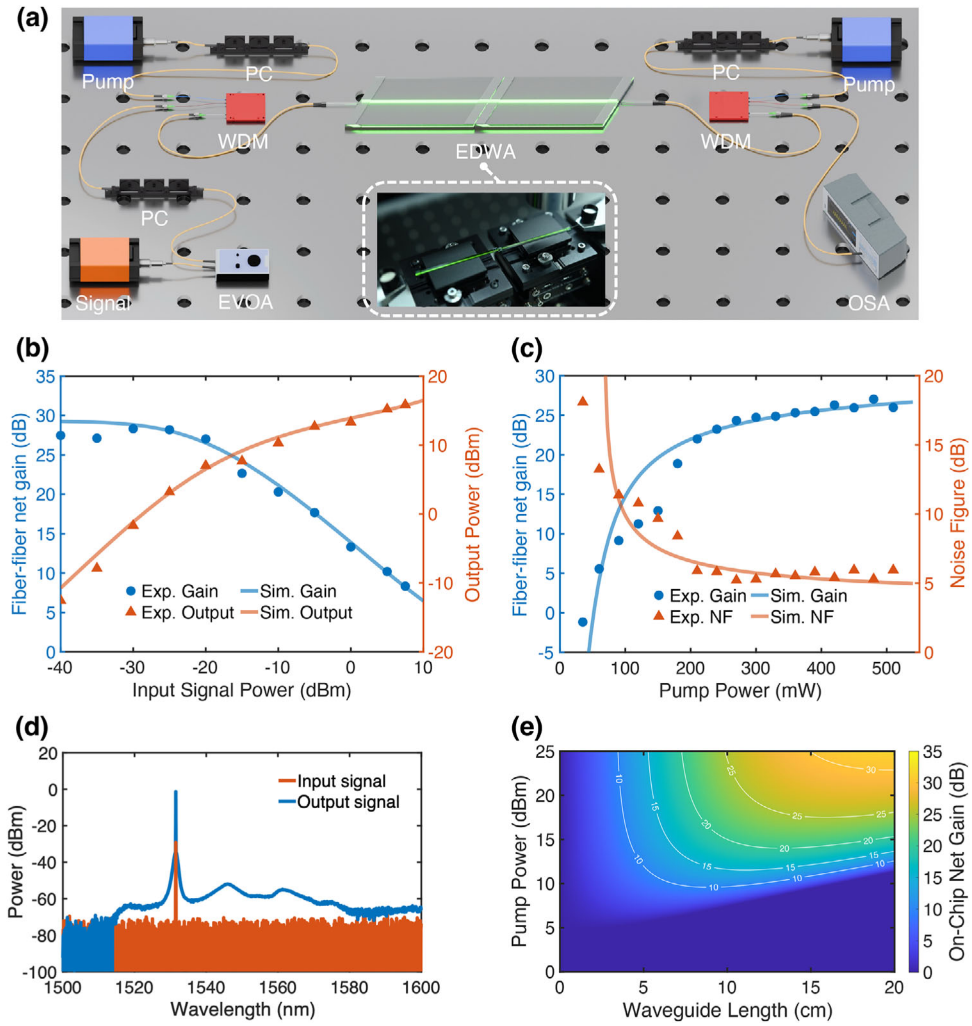

FIGURE 2 | Gain performance characterization of the Er:LNOI waveguide amplifier. (a) Schematic of the experimental setup with bidirectional pumping configuration; inset shows a close-up view of the two Er:LNOI waveguide chips aligned in series. (b) Fiber-to-fiber net gain and output power as functions of input signal power at 1531 nm. Solid lines: simulation; symbols: experiment. (c) Fiber-to-fiber net gain and NF as functions of pump power. Solid lines: simulation; symbols: experiment. (d) Input and output optical spectra at an input signal power of −25 dBm showing 28 dB signal enhancement. (e) Simulated contour plot of on-chip net gain as functions of waveguide length and pump power.

TABLE 1 | Performance Comparison of EDWAs on Different Platforms.

Platform	Peak fiber-to-fiber net gain (dB)	Maximum off-chip output power (dBm)	Length (cm)	Year	Reference
Er:LNOI	>28 (P_{in} = −25 dBm)	15.8 (P_{in} = 7.5 dBm)	11.2	2026	**This work**
Er:TFLN	18.1 (P_{in} = −20 dBm)	>13 (P_{in} = 10 dBm)	8.5	2025	[25]
Er:TFLN	10.5 (P_{in} = −14 dBm)	13.07 (P_{in} = 9.89 dBm)	5.5	2025	[30]
Er:Al_2O_3	>14 (P_{in} = −28.4 dBm)	17.5 (P_{in} ≈ 15 dBm)	30	2025	[31]
Er:Al_2O_3	24.3 (P_{in} = −22 dBm)	17.3 (P_{in} = 16.3 dBm)	50	2025	[32]
Er:TFLN	24.6 (P_{in} = −39.6 dBm)	5 (P_{in} = 0 dBm)	9.16	2025	[24]*
Er:TFLN	3 (P_{in} = −11 dBm)	7.5 (P_{in} = 12 dBm)	7	2025	[33]*
Er:Al_2O_3	10.5 (P_{in} = −17 dBm)	4.1 (P_{in} = 6.4 dBm)	9.31	2024	[34]
Er:LNOI	16.3 (P_{in} = −5.9 dBm)	10.66 (P_{in} = −5.9 dBm)	5.6	2024	[21]*
Er:Si_3N_4	24 (P_{in} = −11.5 dBm)	15.8 (P_{in} = 4.2 dBm)	50	2022	[7]*

*Off-chip net gain is calculated by subtracting the reported coupling loss from the measured on-chip gain.

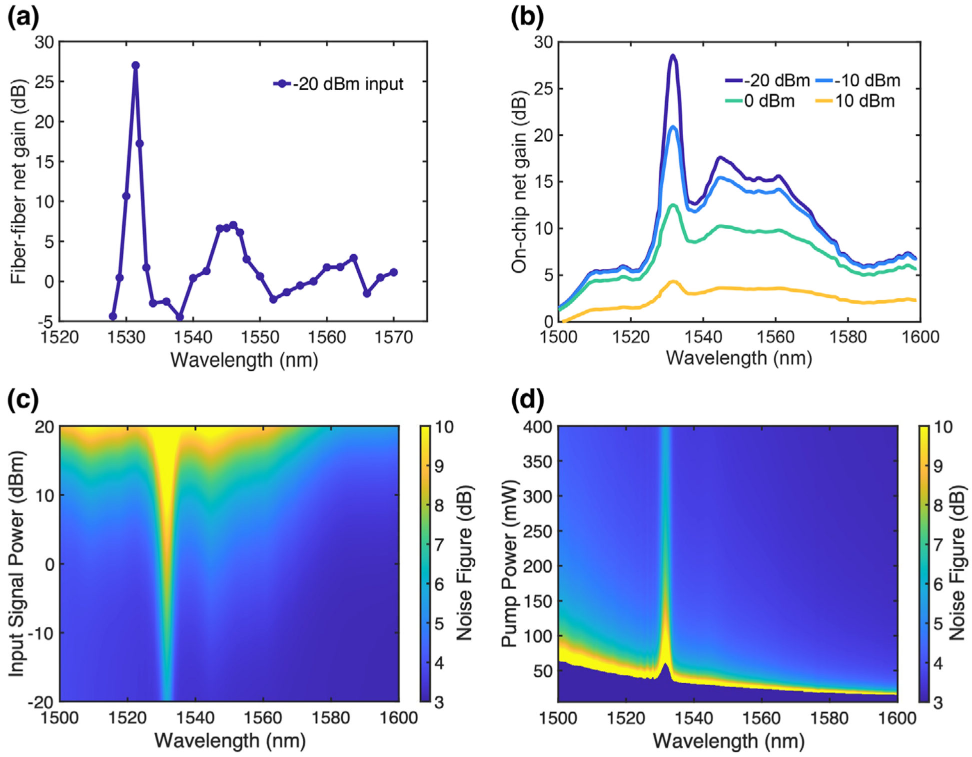

FIGURE 3 | Gain bandwidth characteristics and NF modeling. (a) Measured fiber-to-fiber net gain spectrum across the C-band under 1480 nm pumping with an input signal power of −20 dBm, showing a peak at 1531 nm. (b) Simulated on-chip net gain spectra at various input signal powers from −20 dBm to 10 dBm. (c) Two-dimensional map of simulated NF as functions of wavelength and input signal power. (d) Two-dimensional map of simulated NF as functions of wavelength and pump power.

2.3 | Gain Bandwidth and Noise Figure Modeling

The wavelength dependence of the amplifier gain is investigated experimentally. Figure 3a shows the measured fiber-to-fiber net gain spectrum across the C-band at an input signal power of −20 dBm, exhibiting a pronounced peak around 1531 nm that corresponds to the maximum emission cross-section of erbium ions in lithium niobate. The gain spectrum shows significant wavelength dependence, with the net gain decreasing rapidly away from the peak wavelength and becoming negative at wavelengths where the absorption exceeds the stimulated emission. Figure 3b presents the simulated on-chip net gain spectra at different input signal powers ranging from −20 dBm to 10 dBm, with the connection loss between the two chips excluded. At low input powers, the gain spectrum is dominated by the emission cross-section profile of erbium ions, showing a sharp peak at 1531 nm with a maximum gain exceeding 28 dB. As the input power increases, gain saturation becomes more significant at the peak wavelength, leading to a reduction in peak gain and a relative flattening of the gain spectrum.

The noise performance of the amplifier is characterized through spectral analysis of the ASE. The NF is determined using the optical source subtraction method, which separates the ASE from the amplified signal in the total output power [35]. Based on this approach, the NF can be calculated from the measured optical spectra using:

$$NF = \frac{P_{out} - GP_{sse}}{Gh\nu B_0} + \frac{1}{G}, \tag{1}$$

where P_{out} is the output ASE power at the signal wavelength, G is the fiber-to-fiber net gain on linear scale, P_{sse} is the source spontaneous emission power of the input signal, h is the Planck constant, ν is the optical frequency, and B_0 is the resolution bandwidth of the OSA converted to frequency units via $B_0 = c\Delta\lambda/\lambda^2$.

Among these parameters, P_{sse} is obtained by averaging the background noise floor of the input signal spectrum over a 3 nm bandwidth, excluding 1.5 nm on each side of the signal peak to avoid contamination from the signal itself. The measured P_{sse} is −85.2 dBm at a signal wavelength of 1531.08 nm with an OSA resolution of 0.05 nm. The NF calculation is relatively insensitive to the exact value of P_{sse}. Even when using the extreme values of the noise floor, ranging from −100 dBm to −74.6 dBm, the resulting NF varies by only 0.05 dB.

In contrast, the accurate determination of P_{out} is critical for reliable NF measurement, as small errors in P_{out} can lead to significant variations in the calculated NF. Several approaches have been reported for obtaining P_{out}. One approach exploits the polarization independence of ASE, using a polarization beam splitter to experimentally separate the unpolarized ASE component from the polarized amplified signal [21]. Another approach estimates P_{out} through data processing of the output spectrum, for example using interpolation methods such as shape-preserving cubic interpolation over a wavelength range around the signal peak [25]. In this work, we employ a spectral fitting approach based on the pseudo-Voigt function [35]. This method requires no additional experimental apparatus and derives P_{out} from the fitted spectral line shape, allowing the fitting to use a broader wavelength range with improved accuracy. The measured output spectrum is modeled as the superposition of an ASE background, an amplified signal peak, and a constant offset, i.e., $P_{total}(\lambda) = V_{ASE}(\lambda) + V_{Signal}(\lambda) + C$. Each spectral component is described by a pseudo-Voigt function, a linear combination of Lorentzian $L(\lambda)$ and Gaussian $G(\lambda)$ profiles: $V(\lambda) = A \cdot [\eta \cdot L(\lambda) + (1 - \eta) \cdot G(\lambda)]$. Here, A is the amplitude, and η $(0 \leq \eta \leq 1)$ is the mixing parameter that accounts for the combined effects of homogeneous and inhomogeneous broadening in the erbium emission spectrum. The output ASE power P_{out} is then obtained by evaluating the fitted ASE component at the signal wavelength, yielding $P_{out} = -30.49$ dBm. Substituting all measured parameters into Equation (1) gives an NF of 5.3 dB for the Er:LNOI waveguide amplifier.

The relatively low NF results from strong pumping and high population inversion throughout most of the amplifier length, where the spontaneous emission factor $n_{sp} = \sigma_e(\lambda)N_2/[\sigma_e(\lambda)N_2 - \sigma_a(\lambda)N_1]$ approaches unity as $N_2 \gg N_1$ [36]. Since the NF is related to the spontaneous emission factor by $NF \approx 2n_{sp}$ for an ideal amplifier, the NF approaches the quantum-limited value of 3 dB under these conditions [35].

Figure 3c shows a two-dimensional map of the simulated NF as functions of wavelength and input signal power. Near the gain peak at 1531 nm, the amplifier reaches its maximum fiber-to-fiber net gain, with a corresponding NF of 5.3 dB under the operating condition for maximum gain. Away from this wavelength, particularly around 1520 nm where ground-state absorption is strong, the NF increases substantially due to reduced inversion and enhanced signal reabsorption. At low signal powers below −10 dBm, the NF remains nearly uniform across the gain bandwidth, while at higher input powers the NF increases due to gain saturation effects.

The dependence of NF on pump power is illustrated in Figure 3d, which maps the noise characteristics as functions of wavelength and pump power. The simulations show that sufficient pump power avoiding insufficient population inversion is required to maintain a low NF. Once the pump power exceeds this threshold, the NF stabilizes at low values across most of the C-band, with the minimum approaching 3–4 dB near the emission peak. These results define the pump-power range needed for wavelength-division multiplexing applications, where both high gain and low NF are required across multiple wavelength channels.

2.4 | Suppression of Parasitic Lasing

In high-gain waveguide amplifiers, the Fresnel reflection at the waveguide input and output facets can form an optical Fabry–Pérot (F–P) cavity that leads to parasitic lasing when the round-trip gain exceeds the cavity loss [7]. This parasitic lasing occurs preferentially at wavelengths near the peak of the ASE spectrum, where the gain is highest, and competes with the signal for the available population inversion. As a result, the measured gain at the peak wavelength may be overestimated, and the achievable net gain at the signal wavelength is clamped, limiting the amplifier performance.

Figure 4a shows the ASE spectra of a flat-polished Er:LNOI waveguide under forward pumping at various pump powers from 50 to 200 mW. As the pump power increases, the ASE intensity grows and a sharp peak emerges around 1530 nm, indicating the onset of parasitic lasing in the F–P cavity formed by the waveguide facets. Figure 4b presents the amplified signal spectra at 1530.6 nm under different forward pump powers; this wavelength is deliberately chosen to be 0.8 nm away from the ASE peak to distinguish between signal amplification and parasitic lasing. At low pump power, the signal is amplified normally with a single peak. However, at high pump power, two peaks appear in the spectrum, in which the parasitic lasing peak even exceeds the amplified signal in intensity, indicating that the ASE lasing depletes the population inversion and reduces the gain available for signal amplification.

To suppress the parasitic lasing, we employ angle polishing of the waveguide facets at 5.2° from the normal direction. For flat-polished facets, Fresnel reflection at both facets couples light back into the waveguide mode, forming a resonant F–P cavity that supports parasitic lasing when the gain is sufficiently high. In contrast, for angle-polished facets, the reflected light is directed away from the waveguide core at an angle determined by Snell's law, coupling predominantly into cladding or radiation modes rather than the guided mode. This reduces the modal reflectivity and breaks the F–P cavity feedback, raising the threshold for parasitic lasing and allowing operation at higher gain.

We evaluate the effect of angle polishing by comparing the ASE spectra before and after the treatment under identical pumping conditions. Figure 4c shows the ASE spectra of the same waveguide with flat-polished and angle-polished facets, both measured under bidirectional pumping with 200 mW in each direction. With flat-polished facets, a strong parasitic lasing peak reaching −6.8 dBm is observed at 1531 nm, indicating significant F–P cavity oscillation. After angle polishing, the parasitic lasing is completely suppressed, with the peak power reduced to −55.8 dBm, representing a suppression of approximately 49 dB. The ASE spectrum after angle polishing exhibits a smooth profile without sharp features, confirming the elimination of the F–P cavity feedback.

Figure 4d compares the gain characteristics of waveguides with flat-polished and angle-polished facets. For the flat-polished sample, the fiber-to-fiber net gain increases with pump power initially but saturates early at around 200 mW, reaching a maximum gain of approximately 13 dB. Beyond this point, further increasing the pump power causes the gain to decrease, as the parasitic lasing at the ASE peak wavelength increasingly depletes the population inversion and competes with the signal for gain. In contrast, the angle-polished sample exhibits continuous gain increase with pump power without the gain roll-off observed in the flat-polished case. This behavior confirms that angle polishing effectively suppresses the parasitic lasing, allowing the full population inversion to be utilized for signal amplification and enabling significantly higher net gain operation.

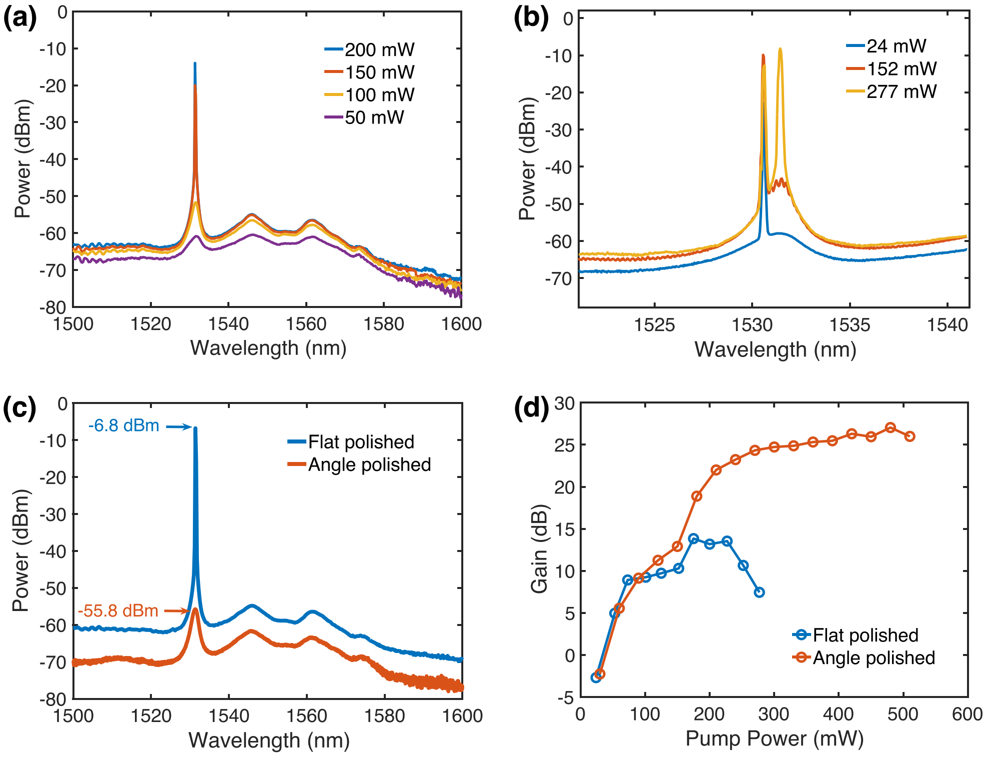

FIGURE 4 | Suppression of parasitic lasing by angle polishing. (a) ASE spectra of a flat-polished Er:LNOI waveguide at pump powers from 50 to 200 mW. (b) Amplified signal spectra at 1530.6 nm under different pump powers, showing the competition between signal amplification and parasitic lasing at high pump power. (c) Comparison of ASE spectra before and after angle polishing under bidirectional pumping with 200 mW in each direction. (d) Fiber-to-fiber net gain as a function of pump power for waveguides with flat-polished and angle-polished facets.

3 | Conclusions

In summary, we have demonstrated an Er:LNOI waveguide amplifier that achieves a record fiber-to-fiber net gain exceeding 28 dB, surpassing all previously reported fiber-to-fiber net gain values among erbium-doped integrated waveguide amplifiers. The amplifier consists of two waveguide segments in series under bidirectional pumping at 1480 nm, delivering an output power exceeding 15 dBm. The device exhibits low NF and high external net gain, with good agreement between experimental results and theoretical modeling. Angle polishing of the waveguide facets effectively suppresses parasitic lasing, enabling stable high-gain operation without gain degradation at high pump powers. The micro-waveguide geometry provides good mode matching with standard lensed fibers and enhanced power handling capability, making this amplifier architecture suitable for practical system integration. Further improvements in performance can be expected through optimized waveguide design with reduced propagation loss, advanced packaging techniques for lower coupling loss, and gain-bandwidth broadening by engineering the local environment of Er ions to enhance the overall gain across the C band. Reducing the refractive-index contrast between the waveguide core and substrate could enable a single-chip spiral gain waveguide, thereby providing a scalable route to longer gain lengths within a compact device footprint. These results establish Er:LNOI micro-waveguide amplifiers as a viable platform for integrated optical amplification in optical communication, sensing, and signal processing.

Acknowledgements

This work was supported by the National Key Research and Development Program of China (2023YFA1407200); National Natural Science Foundation of China (12192252, 12504390); Science and Technology Commission of Shanghai Municipality (24JD1401700); Shanghai Municipal Science and Technology Major Project (2019SHZDZX01-ZX06); Guangdong Provincial Quantum Science Strategic Initiative (GDZX2403003); Quantum Science and Technology-National Science and Technology Major Project (2021ZD0300802); Yangyang Development Fund.

Conflicts of Interest

The authors declare no conflicts of interest.

Data Availability Statement

The data that support the findings of this study are available from the corresponding author upon reasonable request.

References

1. P. C. Becker, N. A. Olsson, and J. R. Simpson, *Erbium-Doped Fiber Amplifiers: Fundamentals and Technology* (Academic Press, 1999).

2. S. B. Poole, D. N. Payne, R. J. Mears, M. E. Fermann, and R. I. Laming, "Fabrication and Characterization of Low-Loss Optical Fibers Containing Rare-Earth Ions," *Journal of Lightwave Technology* 4, no. 7 (1986): 870–876.

3. R. J. Mears, L. Reekie, I. M. Jauncey, and D. N. Payne, "Low-Noise Erbium-Doped Fibre Amplifier Operating at 1.54 μm," *Electronics Letters* 23, no. 19 (1987): 1026.

4. J. D. B. Bradley and M. Pollnau, "Erbium-Doped Integrated Waveguide Amplifiers and Lasers," *Laser & Photonics Reviews* 5, no. 3 (2011): 368–403.

5. D. Zhu, L. Shao, M. Yu et al., "Integrated Photonics on Thin-Film Lithium Niobate," *Advances in Optics and Photonics* 13, no. 2 (2021): 242–352.

6. A. Sobhanan, A. Anthur, S. O'Duill et al., "Semiconductor Optical Amplifiers: Recent Advances and Applications," *Advances in Optics and Photonics* 14, no. 3 (2022): 571–651.

7. Y. Liu, Z. Qiu, X. Ji et al., "A Photonic Integrated Circuit-Based Erbium-Doped Amplifier," *Science* 376, no. 6599 (2022): 1309–1313.

8. S. A. Vázquez-Córdova, M. Dijkstra, E. H. Bernhardi et al., "Erbium-Doped Spiral Amplifiers with 20 dB of Net Gain on Silicon," *Optics Express* 22, no. 21 (2014): 25993–26004.

9. J. Mu, M. Dijkstra, J. Korterik, H. Offerhaus, and S. M. García-Blanco, "High-Gain Waveguide Amplifiers in Si_3N_4 Technology via Double-Layer Monolithic Integration," *Photonics Research* 8, no. 10 (2020): 1634–1641.

10. J. Rönn, W. Zhang, A. Autere et al., "Ultra-High On-Chip Optical Gain in Erbium-Based Hybrid Slot Waveguides," *Nature Communications* 10 (2019): 432.

11. H. C. Frankis, H. M. Mbonde, D. B. Bonneville et al., "Erbium-Doped TeO_2-Coated Si_3N_4 Waveguide Amplifiers with 5 dB Net Gain," *Photonics Research* 8, no. 2 (2020): 127–134.

12. D. Barbier, P. Bruno, C. Cassagnettes et al., "Net Gain of 27 dB with a 8.6-cm-Long Er/Yb-Doped Glass-Planar-Amplifier," in *Optical Fiber Communication Conference* (1998): 45–46.

13. H. Sun, L. Yin, Z. Liu et al., "Giant Optical Gain in a Single-Crystal Erbium Chloride Silicate Nanowire," *Nature Photonics* 11, no. 9 (2017): 589–593.

14. N. Xiong, S. Su, Z. Yan et al., "On-Chip Net-Amplified Modulator in Erbium-Doped Thin-Film Lithium Niobate With 110-GHz Bandwidth," *Photonics Research* 14, no. 5 (May 2026): 2140–2148, https://doi.org/10.1364/PRJ.586899.

15. Y. Jia, J. Wu, X. Sun et al., "Integrated Photonics Based on Rare-Earth Ion-Doped Thin-Film Lithium Niobate," *Laser & Photonics Reviews* 16, no. 10 (2022): 2200059.

16. A. Honardoost, K. Abdelsalam, and S. Fathpour, "Rejuvenating a Versatile Photonic Material: Thin-Film Lithium Niobate," *Laser & Photonics Reviews* 14, no. 9 (2020): 2000088.

17. H. Han, S. Ruan, and B. Xiang, "Heterogeneously Integrated Photonics Based on Thin-Film Lithium Niobate Platform," *Laser & Photonics Reviews* 19, no. 1 (2024): 2400649, https://doi.org/10.1002/lpor.202400649.

18. F. Shen, Z. Mao, W. Fan et al., "OAM Multiplication Operator Enabled Holographic Multiplexing," *Light: Science &and Applications* 15, no. 1 (2026): 18, https://doi.org/10.1038/s41377-025-02107-2.

19. S. Dutta, E. A. Goldschmidt, S. Barik, U. Saha, and E. Waks, "Integrated Photonic Platform for Rare-Earth Ions in Thin-Film Lithium Niobate," *Nano Letters* 20, no. 1 (2020): 741–747.

20. M. Cai, K. Wu, J. Xiang et al., "Erbium-Doped Lithium Niobate Thin Film Waveguide Amplifier With 16 dB Internal Net Gain," *IEEE Journal of Selected Topics in Quantum Electronics* 28, no. 3 (2022): 8200608.

21. M. Cai, T. Li, X. Zhang et al., "Gain Dynamics in Integrated Waveguide Amplifier Based on Erbium-Doped Thin-Film Lithium Niobate," *ACS Photonics* 11, no. 11 (2024): 4923–4932.

22. C. Yan, S. Wang, S. Zhao et al., "A Short High-Gain Waveguide Amplifier Based on Low Concentration Erbium-Doped Thin-Film Lithium Niobate on Insulator," *Applied Physics Letters* 122, no. 12 (2023): 123503.

23. X. Xue, J. Qiu, T. Ding et al., "Integrated Erbium-Doped Waveguide Amplifier on Lithium Niobate on Insulator," *Optical Materials Express* 14, no. 8 (2024): 1985–1994.

24. Y. Wang, B. Wang, B. Shen et al., "Unifying Optical Gain and Electro-Optical Dynamics in Er-Doped Thin-Film Lithium Niobate Platform," *Nature Communications* 16 (2025): 10462.

25. M. Li, J. Yu, Z. Wang et al., "Monolithic Low-Noise Erbium-Doped Thin-Film Lithium Niobate Waveguide Amplifier With 18 dB Fiber to Fiber Net Gain," *ACS Photonics* 12, no. 11 (2025): 6388–6396.

26. Y. Zhang, H. Li, T. Ding et al., "Scalable, Fiber-Compatible Lithium-Niobate-on-Insulator Micro-Waveguides for Efficient Nonlinear Photonics," *Optica* 10, no. 6 (2023): 688–693, https://doi.org/10.1364/OPTICA.489383.

27. L. Agazzi, K. Wörhoff, and M. Pollnau, "Energy-Transfer-Upconversion Models, Their Applicability and Breakdown in the Presence of Spectroscopically Distinct Ion Classes: A Case Study in Amorphous $Al_2O_3 : Er^{3+}$," *Journal of Physical Chemistry C* 117, no. 13 (2013): 6759–6776.

28. J. Huang, R. Li, S. Wang et al., "Polarization-Dependent Gain Characterization in X-Cut LNOI Erbium-Doped Waveguide Amplifiers," *Nanophotonics* 14, no. 27 (2025): 5081–5094, https://doi.org/10.1515/nanoph-2025-0335.

29. E. Desurvire, *Erbium-Doped Fiber Amplifiers: Principles and Applications* (Wiley, 1994).

30. J. Han, M. Li, R. Wu et al., "High Fiber-to-Fiber Net Gain in Erbium-Doped Thin-Film Lithium Niobate Waveguide Amplifier as an External Gain Chip," *Opto-Electronic Science* 4 (2025): 250004-1.

31. C. E. Osornio-Martinez, D. B. Bonneville, M. Dijkstra, and S. M. García-Blanco, "Scalable Erbium-Doped Waveguide Amplifier With External Fiber-to-Fiber Gain Using Reactively Sputtered Polycrystalline Aluminium Oxide," *Optics Express* 33, no. 11 (2025): 22458, https://doi.org/10.1364/OE.558707.

32. C. E. Osornio-Martinez, D. B. Bonneville, M. Dijkstra, A. R. do Nascimento Jr., and S. M. García-Blanco, "Broadband Packaged Erbium-Doped Polycrystalline Al_2O_3 Waveguide Amplifier With 24 dB External Net Gain," *Optics Express* 33, no. 14 (2025): 28985–28994, https://doi.org/10.1364/OE.571485.

33. R. Bao, Z. Fang, J. Liu et al., "An Erbium-Doped Waveguide Amplifier on Thin-Film Lithium Niobate With an Output Power Exceeding 100 mW," *Laser & Photonics Reviews* 19, no. 1 (2025): 2400765, https://doi.org/10.1002/lpor.202400765.

34. H. Zhang, Y. Wang, Y. He et al., "Atomic-Layer Engineered Erbium-Doped Waveguide Amplifier With a 14.4 dB Net Gain," *ACS Photonics* 12, no. 2 (2024): 674–683, https://doi.org/10.1021/acsphotonics.4c01466.

35. J. Lorenzen, N. Singh, K. Wang, S. M. Garcia-Blanco, and F. X. Kärtner, "Silicon Photonics LMA Amplifiers: High Power, High Gain, Low Noise and Tunable Polarization Sensitivity," *Optics Express* 33, no. 3 (2025): 3915–3930.

36. J. Lorenzen, K. Wang, M. Kilinc et al., "Zero-PDG Silicon Photonic Amplifier With High Saturation Power and Low Noise Figure," *Nature Communications* 17, no. 1 (2026): 5670, https://doi.org/10.1038/s41467-026-74486-y.